NRL Memorandum Report 5600

Vortex-Induced Vibrations of Marine Cables and Structures

OWEN M. GRIFFIN

Fluid Dynamics Branch
Marine Technology Division

June 19, 1985

This project was sponsored by the U.S. Department of the Interior, Minerals Management Service, Technology Assessment and Research Branch, Authorization No. 3LA 6035-1037.

NAVAL RESEARCH LABORATORY
Washington, D.C.

SECURITY CLASSIFICATION OF THIS PAGE

REPORT DOCUMENTATION PAGE

1a. REPORT SECURITY CLASSIFICATION UNCLASSIFIED	1b. RESTRICTIVE MARKINGS
2a. SECURITY CLASSIFICATION AUTHORITY	3. DISTRIBUTION / AVAILABILITY OF REPORT Approved for public release; distribution unlimited.
2b. DECLASSIFICATION / DOWNGRADING SCHEDULE	
4. PERFORMING ORGANIZATION REPORT NUMBER(S) NRL Report 5600	5. MONITORING ORGANIZATION REPORT NUMBER(S)
6a. NAME OF PERFORMING ORGANIZATION Naval Research Laboratory 6b. OFFICE SYMBOL (If applicable)	7a. NAME OF MONITORING ORGANIZATION
6c. ADDRESS (City, State, and ZIP Code) Washington, DC 20375	7b. ADDRESS (City, State, and ZIP Code)
8a. NAME OF FUNDING / SPONSORING ORGANIZATION U.S. Department of Interior 8b. OFFICE SYMBOL (If applicable) Min. Mgt. Serv.	9. PROCUREMENT INSTRUMENT IDENTIFICATION NUMBER
8c. ADDRESS (City, State, and ZIP Code) Reston, VA 22091	10. SOURCE OF FUNDING NUMBERS PROGRAM ELEMENT NO. DOI; PROJECT NO.; TASK NO. (327); WORK UNIT ACCESSION NO. DN380-565

11. TITLE (Include Security Classification)
Vortex-Induced Vibrations of Marine Cables and Structures

12. PERSONAL AUTHOR(S)
Griffin, O.M.

13a. TYPE OF REPORT	13b. TIME COVERED	14. DATE OF REPORT (Year, Month, Day)	15. PAGE COUNT
Interim	FROM 10/83 TO 4/85	1985 June 19	25

16. SUPPLEMENTARY NOTATION This project was sponsored by the U.S. Department of the Interior, Minerals Management Service, Technology Assessment and Research Branch, Authorization No. 3LA 6035-1037.

17. COSATI CODES		
FIELD	GROUP	SUB-GROUP

18. SUBJECT TERMS (Continue on reverse if necessary and identify by block number)
Marine cables Marine structures
Hydrodynamic drag Vortex-induced vibrations

19. ABSTRACT (Continue on reverse if necessary and identify by block number)

The dynamic analysis of marine structures and cable systems has become increasingly important in order to predict stress distributions and operational lifetimes in hostile ocean environments. This is largely because the amplitudes of vortex-induced vibration for a cylindrical structure such as a riser or pipeline in water are an order of magnitude greater than for a similar structure in air. The small mass ratio (structure to displace fluid) in water produces small values of the reduced damping which in turn result in the relatively large limiting vibration amplitudes shown in this report.

Risers, platform mooring cables and other long, slender structures often are subjected to spanwise non-uniform shear currents. The response of long cylinders in non-uniform flows cannot be predicted accurately in many cases using existing methods which were originally developed for uniform flows. There is a limited base of data available for current shear effects from both laboratory and field experiments. However, it is

(Continues)

20. DISTRIBUTION / AVAILABILITY OF ABSTRACT	21. ABSTRACT SECURITY CLASSIFICATION
☐ UNCLASSIFIED/UNLIMITED ☒ SAME AS RPT ☐ DTIC USERS	UNCLASSIFIED
22a. NAME OF RESPONSIBLE INDIVIDUAL O.M. Griffin	22b. TELEPHONE (Include Area Code) 202-767-2904 / 22c. OFFICE SYMBOL Code 5841

DD FORM 1473, 84 MAR 83 APR edition may be used until exhausted.
All other editions are obsolete.

SECURITY CLASSIFICATION OF THIS PAGE

19. ABSTRACT (Continued)

possible from these results to make reasonable engineering estimates of the level and extent of vortex-induced vibrations in shear currents. Several examples are given here to illustrate these estimates.

The vortex-induced hydrodynamic drag forces on vibrating structures in water are amplified substantially above the corresponding case of a structure at rest. This drag amplification has been measured in several extensive experiments and reaches 250 percent at the largest amplitudes of crossflow displacement. The available experimental results for circular cylindrical members are summarized here and put to use in several example calculations. This amplification of the hydrodynamic drag forces results in large steady stresses and deflections when the oscillatory stresses and deflections also are highest.

CONTENTS

FOREWORD AND ACKNOWLEDGMENTS

This report was prepared at the Naval Research Laboratory as part of a research program supported by the Minerals Management Service of the U.S. Department of the Interior. I am grateful to a number of colleagues who provided their own results and the results of others, especially Prof. G. Moe of the Norwegian Institute of Technology, Dr. T. Overvik of Statoil (Norway), and Prof. J. K. Vandiver of the Massachusetts Institute of Technology. Mr. Charles E. Smith of the MMS provided continuing cooperation during the course of this program.

MAGNITUDE OF THE PROBLEM

Many types of marine structures are susceptible to vortex-induced vibrations. These include the risers and conductor tubes that are employed in in offshore oil exploration and production, deep water pipelines, members of jacketed structures and mooring cable arrays. Several case studies have been discussed in the literature in recent years. First among these was the installation of an offshore oil terminal at Immingham in the United Kingdom during late 1969. Significant vortex-induced vibrations occurred during the installation of pilings in a tidal flow, and severe construction difficulties were encountered. A wide ranging test program was conducted both at the field sites and in various laboratories in order to determine the causes of the vibrations and to devise means of preventing them.

The underwater installation of 187 m (610 ft) long foundation piles for the Shell Oil production platform in the Cognac field of the Gulf of Mexico presented several potential problems due to vortex-induced vibrations. Currents of sufficient magnitude to cause resonant vibrations of the piles had been measured at the installation site which has a water depth of 350 m (1150 ft). The anticipated problems included the "stabbing" of oscillating piles into sleeves in the platform base, and vibrations of the stabbed piles during the subsequent driving operation. Under certain circumstances a fatigue life of four days was predicted for the bare piles when their exposed length of 130 m (425 ft) was resonantly excited by currents with magnitudes of 0.45 m/s (0.9 kt).

In 1979 the jack-up rig "Offshore Mercury" was drilling for the British Gas Corporation in 61 m (200 ft) of water in the English Channel near the Isle of Wight. Problems were encountered with vibrations of a drill pipe due to vortex shedding. The rig was operating in 1.5 m/s (3 kt) current and the pipe, 610 mm (2 ft) in diameter, was oscillating with a displacement amplitude of $\pm$ 0.5 diameters across to the current direction. Not only was the drill pipe resonantly vibrating, but also drilling machinery on the deck of the rig was vibrating in unison with it. These resonant vibrations caused two fatigue failures of the drill pipe. Prior to the time when an acceptable solution was devised, approximately $5 million in losses were incurred. A photograph of the drill pipe deployed on site is given in Fig. 1.

Laboratory and field tests and design studies were conducted in the early 1980's to develop a riser fairing that would allow a drill ship to operate off the coast of Brazil in 400 m (1330 ft) of water and in

Fig. 1 — Vortex shedding from a drill pipe deployed from the jack-up rig *Ocean Monarch* in the English Channel; from Every and King (8). A helical strake vortex spoiler is wrapped around the pipe. Prior to the installation of the spoiler, two pipe failures had been caused by vortex-induced vibrations.

strong surface currents up to 2 m/s (4 kt). These tests resulted in the development of economical and practical fairing and helical strake devices to suppress the vortex-induced vibrations.

A number of more recent test programs have been conducted or are underway in the offshore industry. Most or all of the results obtained are proprietary to the various participants.

NOTATION

The following symbols are used in this report:

C_D, C_{D0}	Steady drag coefficient on a vibrating (stationary) cylinder or cable.
C_L	Lift coefficient; see Eq. (6).
C_{LE}	Excitation force coefficient; see Eq. (6).
D	Body diameter (m or ft).
f_n	Natural frequency (Hz).
f_s	Strouhal frequency (Hz).
I_l	Modal scaling factor; see Eq. (4).
k_s	Reduced damping; see Eq. (1).
L	Body length (m or ft).
m	Physical mass per unit length (kg/m or lb_m/ft).
m'	Virtual mass (physical plus added mass) per unit length (kg/m or lb_m/ft).
St	Strouhal number, $f_s D/V$.
V	Incident flow velocity (m/s or ft/sec or knots).
V_r	Reduced velocity, $V/f_n D$.

$\bar{x}$	Coordinate measured along the cylinder (m or ft).
w_r	Response parameter, $(1 + 2\bar{Y}/D)\ (V_r \mathrm{St})^{-1}$; see Eq. (8).
$\bar{y}$, $\bar{Y}$	Cross flow displacement, displacement amplitude (m or ft).
Y	Normalized displacement amplitude, $\bar{Y}/D$.
$Y_{\mathrm{EFF,MAX}}$	Normalized displacement amplitude; see Eq. (4).
$\bar{z}$	Coordinate measured in the in-line or mean flow direction (m or ft).
$\bar{\beta}$	Shear flow steepness parameter.
δ	Log decrement of structural damping; see Eq. (1).
γ_i	Normalizing factor; see Eq. (4).
ϕ	Phase angle (deg. or rad); see Eq. (6).
μ	Mass ratio, see Eq. (2).
ν	Kinematic fluid viscosity (m^2/sec or ft^2/sec).
ρ	Fluid density (kg/m^3 or lb_m/ft^3).
$\psi_i(z)$	Mode shape for i th flexible beam mode; see Eq. (3).
ζ_s	Structural damping ratio; see Eq. (2).

VORTEX-INDUCED VIBRATIONS OF MARINE CABLES AND STRUCTURES

1. INTRODUCTION AND BACKGROUND

A common mechanism for resonant, flow-induced vibrations is the organized and periodic shedding of vortices as an incident flow separates alternately from opposite sides of a long, bluff body. These vortices result in steady and unsteady drag forces in line with the flow and unsteady lift or side forces perpendicular to the flow direction. If the structure is flexible and lightly damped internally, then resonant oscillations can be excited normal or parallel to the incident flow direction. For the more common cross flow oscillations, the body and the wake usually oscillate in unison at a frequency near one of the characteristic frequencies of the structure. The shedding meanwhile is shifted away from the natural, or Strouhal, frequency at which pairs of vortices would be shed if the structure were restrained from vibrating. This phenomenon is known as "lock-on" or "wake capture."

The vortex-induced vibrations of marine cables, commonly termed *strumming*, result in increased steady and unsteady hydrodynamic forces, and amplified acoustic flow noise. They sometimes lead to early fatigue, structural damage and to failure. These flow-excited oscillations very often are a critical factor in the design of marine cable arrays, riser systems, and offshore pipelines. In air, chimney stacks, jack-up rig legs, high-tension power lines and bus-bars commonly vibrate due to vortex shedding.

The dynamic analysis of marine structures and cable systems both in air and in water has become an important consideration in the prediction of stress distributions and fatigue lives. Reliable experimental data are now reasonably available in the open literature for the dynamic response characteristics and flow-induced forces on a model scale. Based upon these experiments, semi-empirical prediction models have been developed and favorably compared with field test data under limited conditions.

2. BASIC CHARACTER OF VORTEX SHEDDING

The frequency f_s of the vortex shedding from a circular cylinder member such as a cable or a riser is related to the other main flow parameters (D, the diameter of the cylinder; V, the flow velocity) through the nondimensional Strouhal number which is defined as

Manuscript approved April 18, 1985.

$$St = \frac{f_s D}{V}.$$

The value of the Strouhal number varies somewhat in different regimes of the Reynolds number and with the shape of the cylinder (circular, D-section, triangular, etc). For the range of the Reynolds number where the Strouhal number remains constant the relation between the shedding frequency and the velocity is linear for a given cylinder, i.e.,

$$f_s = KV,$$

where $K = St/D$. If a cylinder immersed in a flowing fluid is free to vibrate in the cross-flow and in-line directions, then the latter relation does not hold in the vicinity of the natural frequency of the cylinder. This resonance phenomenon—called "lock-on" or "wake capture"—is discussed in this report.

If the Reynolds number is lower than about 10^5, then the vortex shedding is predominantly periodic and the value of the Strouhal number can be assumed to be about $St = 0.2$ for a circular cylinder or cable. Measurements of the frequencies, displacement amplitudes and forces which result from vortex-induced vibrations have been obtained by many investigators from experiments both in air and in water. The basic aspects of the problem of vortex-induced vibrations in general have been reviewed recently by Sarpkaya (1) and Bearman (2). King (3), and Griffin and Ramberg (4,5) have discussed the subject in the context of marine applications.

3. AMPLITUDES OF DISPLACEMENT

It has been shown by numerous investigators (see References 1, 3 and 4, for example) that the displacement amplitude is a function primarily of a response or "reduced damping" parameter of the overall form

$$k_s = \frac{2m\delta}{\rho D^2}. \tag{1}$$

The formulation of the reduced damping also is often written in the analogous form

$$\zeta_s/\mu = 2\pi\ St^2 k_s \tag{2}$$

when the damping is small and $\zeta_s = \delta/2\pi$. The importance of the reduced damping follows directly from resonant force and energy balances on the vibrating structure. It is important to note that the damping coefficients ζ_s and δ represent the damping measured in *still air*. For all practical purposes this is then equivalent to in vacuo structural damping. Moreover, the relation between Y_{MAX} and k_s or ζ_s/μ holds equally well for flexible cylindrical members with normal mode shapes given by $\psi_i(z)$, for the i th mode.

If the cross flow displacement (from equilibrium) of a flexible structure with normal modes $\psi_i(z)$ is written as

$$y_i = Y\psi_i(z) \sin \omega t \tag{3}$$

at each spanwise location z, then the peak amplitude of displacement can be scaled by the factor

$$Y_{EFF,MAX} = YI_i^{1/2}/|\psi_i(z)|_{MAX} = Y/\gamma_i, \; Y = \bar{Y}/D, \tag{4a}$$

where

$$I_i = \frac{\int_0^L \psi_i^4(z)\, dz}{\int_0^L \psi_i^2(z)\, dz}, \tag{4b}$$

and

$$\gamma_i = \frac{|\psi i(z)|_{MAX}}{I_i^{1/2}}. \tag{4c}$$

The effective displacement amplitude Y_{EFF} is derived from scaling factors derived from the so-called "wake oscillator" formulation for modelling vortex-induced vibrations (6,7).

Experimental data for Y_{EFF} as a function of ζ_s/μ are plotted in Fig. 2. These results encompass a wide range of single cylinders of various configurations and flexure conditions at Reynolds numbers from 300 to 10^6. For *all* of the data points plotted in Fig. 2 the damping coefficients ζ_s and/or δ were measured in *still air*. This should minimize any further misconceptions among other investigators who have discussed earlier versions of this figure. The various types of structures represented by the data points available through 1982 are given by Griffin and Ramberg (4). As examples, the crossflow vibrations of flexible cantilevers and cylinders in the fundamental mode have been measured under a variety of conditions. Peak-to-peak displacements as great as two and more diameters in water were measured for length/diameter ratios up to about $L/D = 250$. All experiments conducted to date indicate that the limiting displacement amplitude for a flexible circular cylinder is about $Y_{EFF} = \pm 1$ (or slightly greater) at the lowest values of reduced damping.

The most recent measurements in water (see Table 1) shown in Fig. 2 have been made by Every and King (8), Moe (9), and Tsahalis (10,11). These data provide additional confirmation of the earlier trends shown in the figure. It is interesting to note that the reduced damping can increase from $\zeta_s/\mu = 0.01$ to 0.5 (a factor of *fifty*) and the displacement amplitude decreases only from two or three diameters to one diameter (a nominal factor of only *two or three*). This is why it is difficult to suppress the in-water oscillations by means of mass and damping control. Recent discussions of the suppression of vortex-excited oscillations in water are given by Every, King and Griffin (8,12) and by Zdravkovich (13).

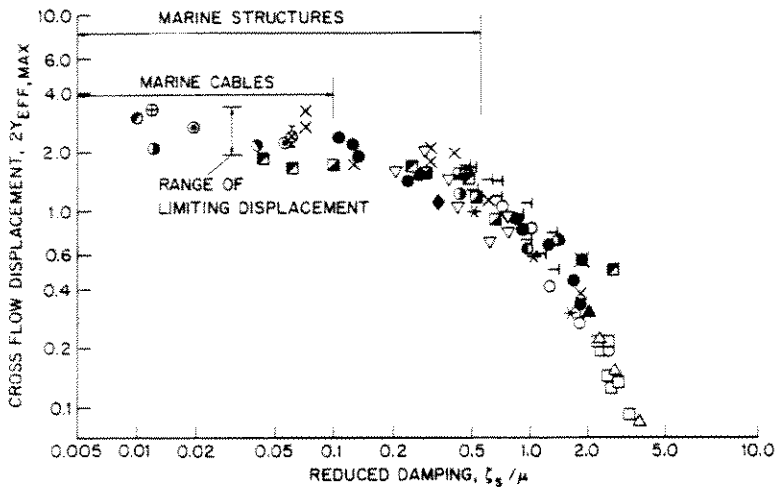

Fig. 2 — The maximum cross flow displacement amplitude, $2Y_{EFF,MAX}$, of circular cylindrical members, scaled as in Eq. (4), as a function of the reduced damping, $\zeta_s = 2\pi St^2 k_s$. The complete legend for the data points is given in Ref. (4), except for the most recent data described in Table 1.

Table 1

Vortex-Induced Vibrations of Circular Cylinders in Water;

New Data Added to Fig. 2

Symbol	Type of Cylinder	Medium	Investigator(s)
◑	Cantilever beam, $L/D = 38$ (76% in water)	Water	Every and King (1979).
⊙	Spring-mounted rigid cylinder, $L/D \cong 20$	Water	Moe(1983)
⊕	Pinned-pinned beam, $L/D = 112$	Water	Tsahalis (1985)

The situation is somewhat different in air as shown in Fig. 3, which has been adapted from Adami and Batch (14). The vibrations of a slender circular cylinder ($L/D = 114$) were measured in a wind tunnel with different end fixities. For the conditions tested the vibrations were nearly independent of the mode, end conditions and the aspect ratio (14). The solid line drawn in the figure is the prediction

$$\overline{Y}_{MAX}/D = \frac{1.29\,\gamma_i}{[1 + 0.43\,(4\pi\,St^2 m\delta/\rho D^2)]^{3.35}}. \qquad (5)$$

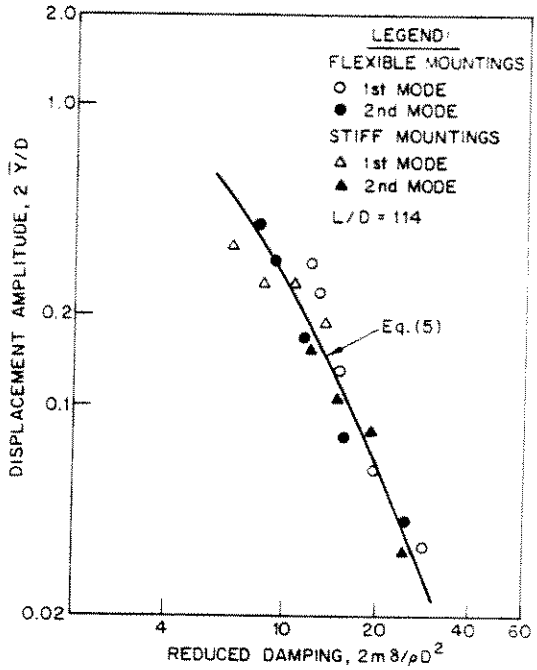

Fig. 3 — The cross flow displacement amplitude, $2\overline{Y}/D$, for flexible circular cylinders in a wind tunnel as a function of the reduced damping, $k_s = 2m\delta/\rho D^2$; adapted from Adami and Batch (1981).

This is a least-squares fit to the data in Fig. 3 which were available in 1977. Other essentially identical prediction curves derived by different methods have been proposed by Sarpkaya (1), Iwan (7) and Blevins (15). The data plotted in Fig. 3 are typical of those obtained in air and would fall toward the right-hand side of Fig. 2. In that region the displacement amplitude is strongly dependent on the reduced damping. Control of the mass and damping of the member then provides a means for suppressing the vibrations. The legs of jack-up drilling rigs under tow and above-ground suspended pipelines are but two examples of the importance of considering the vortex-induced vibrations of long cylinders in air.

These results have been obtained both in air and in water, even though the mass ratios of vibrating structures in the two media differ by two orders of magnitude. For typical structures vibrating in water the mass ratio $\frac{m}{\rho D^2}$ varies from slightly greater than 1 to about 5; in air the mass ratios corresponding to Figs. 2 and 3 typically vary from $\frac{m}{\rho D^2} = 15$ to 500.

4. LIFT OR SIDE FORCES

The resultant unsteady fluid force which acts on a resonantly vibrating, cylindrical structure due to vortex shedding can be divided into several components (16), which are:

- An exciting component of the lift force, in phase with the structure's vibrational velocity, by which energy is transferred to the structure;
- A reaction, or damping force, which is exactly out-of-phase with the structure's velocity;
- An "added mass" force, which is exactly out-of-phase with the structure's acceleration; and
- A flow-induced inertial force.

These various contributions to the total force can be deduced from the total hydrodynamic force as reported, say, by Sarpkaya (1) or the various components can be measured individually (see Ref. 16). The present brief discussion will deal essentially with the exciting force which drives the vibration.

The exciting force coefficient force is defined as

$$C_{LE} = C_L \sin \phi \tag{6}$$

and is important because it is the component of the total force that transfers energy to the vibrating structure. Here ϕ is the phase angle between the hydrodynamic force coefficient C_L and the displacement of the structure. A relatively large number of measurements of C_{LE} by various means are plotted against the effective displacement amplitude Y_{EFF} in Fig. 4. Table 2 summarizes the various conditions under which the experimental results were obtained. There is some scatter in the various measured values of C_{LE}, but certain trends are clear. First there is a maximum of the excitation force coefficient at a peak-to-peak displacement amplitude of between 0.6 and 1 diameters for all the cases shown in the figure. Second, the maximum of the force coefficient is approximately $C_{LE} = 0.5$ to 0.6 for all but one case; the single exception is the result of $C_{LE} = 0.75$. C_{LE} then decreases toward zero and this disappearance of the exciting force results in the limiting effective displacement amplitude. This limiting amplitude is clearly shown at the lowest values of reduced damping in Fig. 2.

5. DRAG FORCES

5.1 Previous Results. An important consequence of the resonant cross flow oscillations of structures and cables due to vortex shedding is an amplification of the mean steady drag force (or equivalently the drag force coefficient C_D). The drag amplification measurements which had been made under a variety of conditions prior to 1980 have been summarized by Griffin and Ramberg (4) as

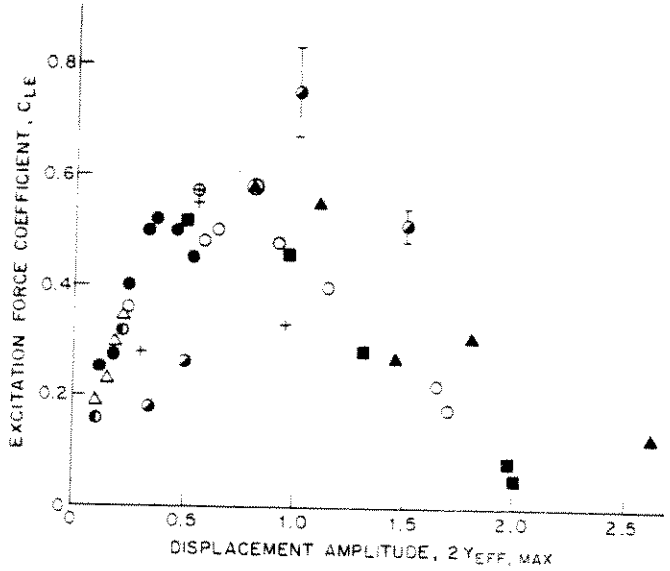

Fig. 4 — The component, C_{LE}, of the lift force plotted against the displacement amplitude $2Y_{EFF,MAX}$, scaled as in Eq. (4). The legend for the data points is given in Table 2.

Table 2
The Excitation Force Coefficients on Vibrating Bluff Cylinders; Description of the Data in Fig. 4

Symbol	Type of cylinder	Medium	Cylinder material	Investigator(s)
▲	Flexible cantilever	Water	PVC	King (1977)
■			PVC Aluminum Stainless steel	
○	Pivoted rigid cylinder	Water & Air	Brass	Vickery and Watkins (1964)
+	Spring-mounted rigid cylinder	Air	Aluminum tubing	Griffin and Koopmann (1977)
◑	Rigid cylinder, forced oscillations	Water	Aluminum tubing	Sarpkaya (1978)
Δ	Flexible cantilever	Air	Aluminum	Hartlen, Baines and Currie (1968)
●	Flexible cylinder	Air	—	Farquharson and McHugh (1956)†
◐	Rigid cylinder forced oscillations	Air	Brass	Simmons and Cleary (1979)

†Quoted by Simmons and Cleary (17).

shown in Fig. 5. A step-by-step method for employing these measurements in the analysis of marine cable structures was developed by Skop, Griffin and Ramberg (19). One step in the method uses Eq. (5) to predict the cross flow displacement amplitude of the member. Measurements of the drag coefficient more recent than those discussed by Griffin and Ramberg are presented in this section of the report.

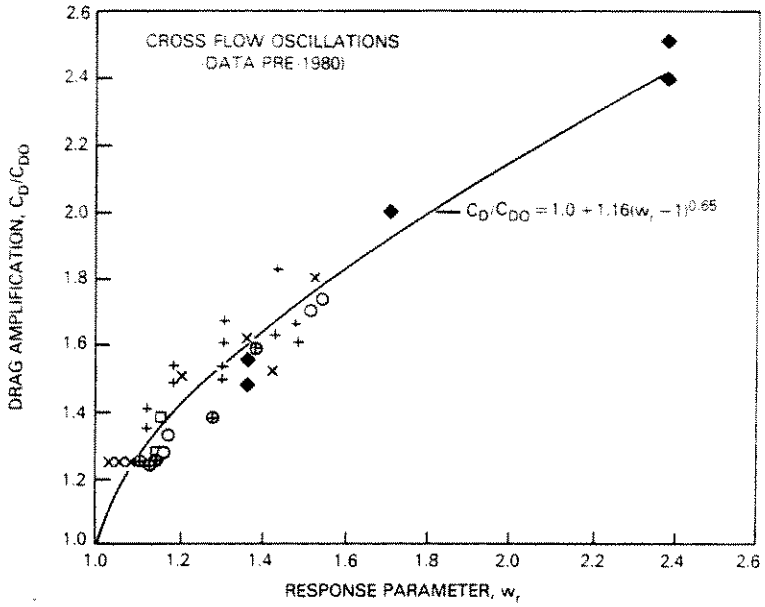

Fig. 5 — The drag coefficient amplification, C_D/C_{D0}, plotted as a function of the wake response parameter, $w_r = (1 + 2\bar{Y}/D)\ (St\ V_r)^{-1}$ for the cross flow vibrations of a circular cylinder; from Skop, Griffin and Ramberg (19).

Measurements of the vortex-induced cross flow vibrations of model marine piles were made by Fischer, Jones and King (20,21). The steady deflection at the free end of the model pile also was measured; in this case the model was a simple, uniform cantilever beam with no tip masses, fully immersed in water, and normal to the incident flow. For low flow velocities the measured and predicted tip deflections coincided when the pile was effectively stationary. The deflection was predicted by assuming a uniform loading

$$w(x) = 1/2\ \rho\ V^2 D C_D(x) \tag{7}$$

over the length of the flexible beam in which the drag coefficient $C_D(x)$ was a constant, $C_D = 1.2$.

When the critical flow velocity for the onset of the vortex-induced vibrations was exceeded, the measured steady deflections in line with the flow departed significantly from the predicted reference curve. Flow velocities above the threshold value caused steady deflections of up to twice the model's

value predicted by assuming $C_D = 1.2$. At the higher values of relative density of the model structure to the density of water, the steady deflections of the model diverged from the predicted curve, reached a maximum and then returned to the predicted curve obtained with $C_D = 1.2$. The pile tip was deflected in line about $\bar{Z} = 1.3$ D at a water velocity V of 0.6 kt (0.3 m/s) when the cross flow displacement amplitude was $\bar{Y} = \pm 1.5$ D. When the pile was restrained from oscillating, the steady in-line deflection of the tip was predicted to be 0.6 D at the same flow velocity. Two related examples are given in Section 7 of this report.

5.2 New Experimental Results. The steady vortex-induced drag coefficient C_D on a freely-oscillating, spring-mounted cylinder is plotted against the reduced velocity V_r in Fig. 6. The measurements were made by Overvik (22) as a baseline case in a more extensive study of the effects of vortex shedding on marine risers. The drag on the cylinder clearly undergoes a resonant-like behavior in much the same manner as the cross flow displacement amplitude. Comparable measurements by Overik of the displacement amplitude $\bar{Y}/D$ track directly the behavior of the drag coefficient C_D. At the peak value of the response, $\bar{Y} \sim \pm 1.1\ D$, the drag coefficient is $C_D = 2.5$. This is an amplification of about 250 percent, which is of sufficient magnitude to cause serious problems for the designer of marine structural members of cylindrical cross section. Less severe problems occur in air because of the smaller vibration amplitudes which are common there.

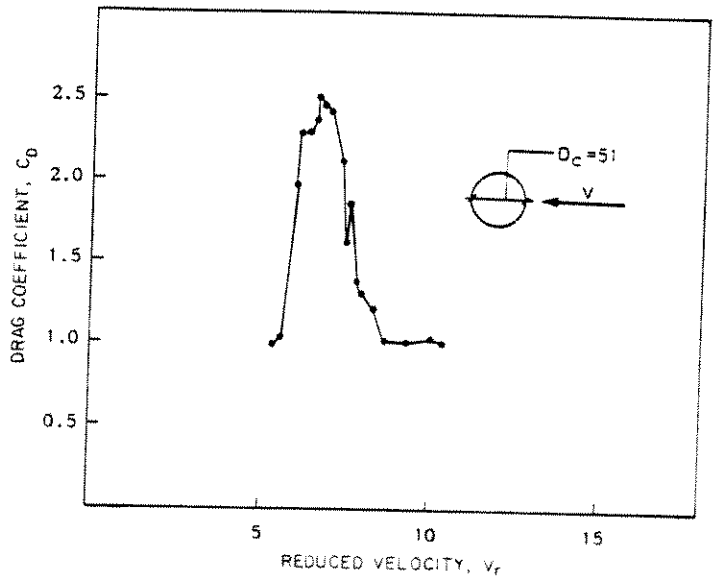

Fig. 6 — The drag coefficient, C_D, plotted against the reduced velocity, V_r, for a spring-mounted circular cylinder; from Overvik (1982). Peak cross flow displacement amplitude, $\bar{Y} = \pm$ 1 to 1.1D.

The drag amplification C_D/D_{D0}, where C_{D0} is the drag coefficient for the stationary cylinder, from a variety of recent experiments is plotted in Fig. 7 as a function of the "wake response" parameter

$$w_r = (1 + 2\ \bar{Y}/D)\ (V_r St)^{-1}. \tag{8}$$

This parameter was proposed by Skop, Griffin and Ramberg (19) and was employed previously as shown in Fig. 5 to correlate the drag amplification that accompanies vortex-induced vibrations. In the particular form shown the factor St^{-1} acts to correct for any variations in Strouhal number (and Reynolds number) among the various experiments. All of the data in Fig. 7 refer to conditions of lock-on between the vortex and vibration frequencies.

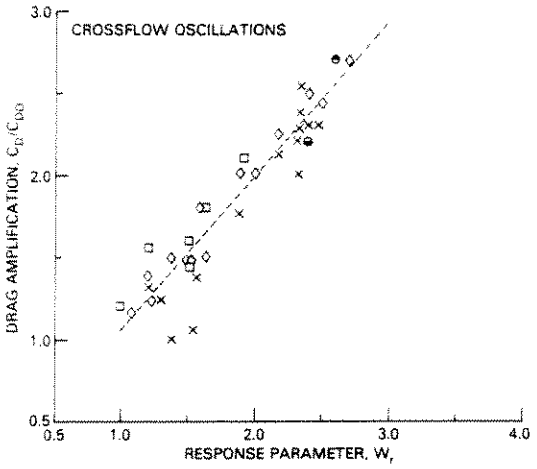

Fig. 7 — The drag coefficient amplification, C_D/C_{D0}, plotted as a function of the wake response parameter, $w_r = (1 + 2\bar{Y}/D)\ (St\ V_r)^{-1}$, for the cross flow vibrations of a circular cylinder. The legend for the data points is given in Table 3.

Table 3
Drag Force Amplification on Vibrating Circular Cylinders; Description of the Data in Fig. 7

Symbol	Medium	Type of Vibration	Investigator(s)
◇	Water	Cross flow, forced	Sarpkaya (1977)
□	Water	Cross flow, forced	Schargel (1980)
X	Water	Cross flow, free	Overvik (1982)
◓, ◒	Water	Cross flow, free	Moe (1982)

It is interesting to note the variety of data which are so well correlated in the figure. The drag measurements from Sarpkaya (23) and Schargel (24) were made on forced-vibrating cylinders in water. Moe (9) and Overvik (22) measured the drag on a freely-vibrating cylinder in water. All of these different experiments resulted in substantial amplifications of the drag coefficient, with $C_D/C_{D0} > 2$ not uncommon for both the free and forced vibrations. The data from Sarpkaya (23) in Fig. 7 are the same as those in Fig. 5. They have withstood well several years of scrutiny.

The dashed line in Fig. 7 is the least-squares fit to the data, given by

$$C_D/C_{D0} = 0.124 + 0.933\ w_r. \tag{9}$$

This is simpler than the result in Fig. 5 but, based on a statistical analysis of several exponential and polynomial representations, it is the best overall representation of the data. Also, the data in Fig. 7 constitute a more extensive base, over a more realistic range of Reynolds numbers, than the data shown in Fig. 5. Use of Eq. (9) therefore is recommended for future applications. Some examples are given later in the report.

Schargel also measured the drag coefficient on a cylinder which was forced to vibrate under non-sinusoidal conditions. When the forcing signal was random with a peak near the expected shedding frequency there was no resonant lock-in and the amplification C_D/C_{D0} of the drag coefficient was reduced in magnitude from the comparable resonant vibration, sinusoidal condition.

Similar levels of hydrodynamic drag amplification to those in Figs. 5 and 7 were measured during the recent field experiments reported by Vandiver and Griffin (25,26). Both a 23 m (75 ft) long pipe segment and a cable with and without attached masses underwent large-amplitude vibrations ($\overline{Y} \sim \pm\ 1D$) due to vortex shedding in a tidal current. Mean drag coefficients of $C_D = 2.4$ to 3.2 were measured during the time intervals when the pipe and cable were strumming at these large amplitudes. In another recent series of experiments Davies and Daniel (27) measured the strumming vibrations of submersible umbilical cables. The model cable of L/D = 100 to 300, which was tested in a large water channel, consistently was excited into large-amplitude cross flow oscillations which were comparable in level to those reported by Vandiver and Griffin. Consequently the normal mean drag coefficients measured by Davies and Daniel were in the range $C_D = 2.5$ to 3.4. This is an amplification factor of 2 to 2.8.

6. EFFECTS OF CURRENT SHEAR

Most of the available experimental data relevant to the vortex-induced vibrations of marine structures and cable systems pertain to uniform incident flows. However, risers, platform mooring cables

and other long slender structures in deep water often are subjected to non-uniform shear current profiles. The response of long cylinders in non-uniform flows cannot be predicted accurately in many cases using existing techniques and data bases.

Recently the general problem of the shear flow about bluff bodies has been addressed in some detail (28). Even on a laboratory scale the reliable data base is relatively sparse for stationary bluff bodies and even less so for those which vibrate. The aspect ratios of the cylindrical bodies investigated thus far have been limited to L/D's at and below 100. Risers, for example, in deep water have typical aspect ratios of L/D = 250 to 2500 (29,30). A recent field study was conducted to assess the vortex-induced response and drag characteristics for a long cable deployed in a vertical shear current (31, 32). The aspect ratios of the cables employed in the experiments were varied up to a maximum of L/D = 1.5 (10^5) in one case (D = 4.1 mm) and of L/D = 1.15 (10^6) in another (D = 2.4 mm). It is apparent from the studies just mentioned that a good dial of empiricism and extrapolation is required in any assessment of shear current effects.

Early studies of shear flow past bluff bodies demonstrated the potential importance of characterizing the nonuniform flow in terms of a "steepness of shear parameter" for the incident velocity gradient. The steepness parameter now is usually defined by

$$\bar{\beta} = \frac{D}{\bar{V}_{\mathrm{REF}}} \frac{d\bar{V}}{d\bar{x}}$$

in the coordinates used in this paper, with $\bar{x}$ measured in the spanwise direction. The reference velocity $\bar{V}_{\mathrm{REF}}$ is the mid-span value in most cases (28). Experiments reported by Fischer, Jones and King (20,21) were conducted to study problems anticipated during the installation of foundation piles for the Cognac platform in the Gulf of Mexico. It is clear from their results that a shear flow with $\bar{\beta}$ = 0.01 to 0.015 had virtually no effect on the anticipated vortex-induced vibrations as compared to uniform flow results obtained under similar conditions ($\bar{Y} = \pm 1$ to 1.5 D). Shear levels such as these were expected from site measurements and were accurately modelled in laboratory-scale experiments.

The natural frequencies of a member such as a riser or piling are relatively wide-spaced, i.e. $f_{n2} = 5f_{n1}$ for example, and vortex lock-on is likely to occur over the two-to-one range of incident current speeds which is characteristic of vortex-induced vibrations in a single mode. When the adjacent frequencies are closely spaced, as in the long cable experiments reported by Kim et al (31, 32), the shear current effects are more random in nature.

It is possible, as described in Ref. 33, to predict the extent of lock-on or the lack of it in a shear current for a slender bluff body. The method to be outlined is dependent upon several assumptions:

(i) The structure or cable has a high ratio, that is $L/D > 20$ or more;

(ii) The *local* Strouhal number is constant or varies only slightly;

(iii) The velocity profile of the shear is linear or nearly so;

(iv) The shear parameter $\bar{\beta}$ is limited to moderate values, that is, $\bar{\beta} < 0.03$.

The first assumption is necessary to insure that the effects of end boundaries and the vortex shedding cells which are common at the ends of a cylinder are negligible. Only cylinders with these large L/D's have regions of vortex shedding that are free of end cell effects. Assumptions (ii) and (iv) are derived from available results in the practical range of shear flows as discussed by Griffin (28, 33). On the basis of these results an approach can be taken as follows. The local Strouhal number is

$$St = \frac{f_S D}{V}$$

or, equivalently

$$St_M = \frac{f_S D}{V_M} = St\left(\frac{V}{V_M}\right) = St\left(1 + \left(\frac{\bar{x}}{D}\right)\bar{\beta}\right). \tag{10}$$

Here the subscript M denotes quantities measured halfway along the cylinder. At the high velocity end of the lock-on region,

$$St_M|_2 = St\left(1 + \frac{\bar{x}_2}{D}\bar{\beta}\right) \tag{11a}$$

and at the low velocity end

$$St_M|_1 = St\left(1 + \frac{\bar{x}_1}{D}\bar{\beta}\right) \tag{11b}$$

where local values of the displacement $\bar{x}$ are used. If the reduced velocity $V_{rM} = V_M/fD$ is introduced, then

$$V_{rM}^{-1}\left(\frac{f_S}{f}|_2 - \frac{f_S}{f}|_1\right) = St\bar{\beta}\left(\frac{\bar{x}}{D}|_2 - \frac{\bar{x}}{D}|_1\right) \tag{12}$$

is obtained when Eq. (11b) is subtracted from Eq. (11a). Simplifying the terminology,

$$V_{rM}^{-1}\Delta\left(\frac{f_S}{f}\right)_{2-1} = St\bar{\beta}\left(\frac{\Delta\bar{x}}{D}\right)_{2-1}. \tag{13}$$

The specific application of Eq. (13) to the case of a flexible cable can be derived easily. If the cable of length L and phase velocity c_P has the natural frequency (in water) f_{nj} in the jth natural mode, then the wavelength λ_j of the vibration is

$$\lambda_j = \frac{c_P}{f_{nj}} = \frac{2L}{j} = \frac{1}{f_{nj}}\sqrt{\frac{T}{m'}} \tag{14}$$

where T is the tension and m' is the virtual (physical + added) mass per unit length of the cable. The shear parameter $\bar{\beta}$ for a linear shear flow can be reduced to the form

$$\bar{\beta} = \frac{D}{V_M}\frac{dV}{d\bar{x}} = \frac{D}{V_M}\frac{\Delta V}{\Delta\bar{x}} = \left(\frac{D}{L}\right)\frac{\Delta V}{V_M} \tag{15}$$

when the length scale $\Delta\bar{x}$ is equal to L and ΔV is the difference in current velocity between the two ends of the cable. Equation (13) can be rearranged into the form

$$\frac{\Delta\bar{x}_{2-1}}{\lambda_j}\left(\frac{\lambda_j}{D}\right) = \Delta\left(\frac{f_S}{f}\right)_{2-1}\frac{1}{St\bar{\beta}\left(\frac{V_M}{fD}\right)}, \tag{13a}$$

which reduces to

$$\frac{\Delta\bar{x}_{2-1}}{\lambda_j} = \Delta\left(\frac{f_S}{f}\right)_{2-1} St^{-1}\left(\frac{f_{nj}L}{\Delta V}\right)\frac{D}{\lambda_j}$$

when Eq. (15) is substituted. This further reduces to

$$\frac{\Delta\bar{x}_{2-1}}{\lambda_j} = \Delta\left(\frac{f_S}{f}\right)_{2-1} St^{-1}\left(\frac{L}{D}\right)\left(\frac{f_{nj}^2D^2}{\Delta V}\sqrt{\frac{m'}{T}}\right) \tag{16}$$

when the cable frequency relationship, Eq. (14), is introduced. From this equation the potential spanwise extent of lock-in can be estimated from the shear current characteristics, a desired cable frequency, and the cable's physical and operational parameters. When the estimated Δx is many wavelengths the probability of sustained resonant cable vibration is small. The *local* Strouhal number St for a slender bluff body deployed in a spanwise shear flow is nearly constant at $St = 0.20$ to 0.22 and $\Delta\left(\frac{f_S}{f}\right)_{2-1} = 0.7$ for $\bar{Y} > 0.1$, based upon available experiments conducted thus far (28, 33).

Equation (16) can be simplified further for marine applications. Assume that $\Delta(f_S)_{2-1} = \Delta f$, the bandwidth of frequencies excited; that $f = f_{nj}$, the jth cable frequency; and that $\Delta\bar{x} = L$, the length of the cable which acts like a taut string. Then Eq. (16) reduces to

$$\frac{L}{\lambda_j} = \left(\frac{\Delta f}{St}\right)\left(\frac{f_{nj}D}{\Delta V}\right)\left(\frac{1}{2f_1}\right)$$

since $\sqrt{\frac{T}{m'}} = 2Lf_1$. The modal density of the natural frequencies for a taut string is

$$n_f = \frac{1}{f_1} \tag{17}$$

and $c_P = \lambda_j f_j$, so that Eq. (16) becomes

$$St\left(\frac{\Delta V}{c_P}\right)\left(\frac{2L}{D}\right) = n_f \Delta f.$$

The number of cable frequencies excited within the bandwidth of frequencies Δf, and correspondingly within the shear current bandwidth ΔV, can be defined as

$$N_S = n_f \Delta_f = St\left(\frac{\Delta V}{c_P}\right)\left(\frac{2L}{D}\right). \tag{18}$$

This equation recently was proposed by Kim, Vandiver and Holler (31, 32). As shown here, Eq. (18) can be derived directly from the characteristic parameters which govern shear current effects on bluff bodies. Equation (13) thus can be adapted for use in predicting current shear effects on other marine structures such as risers, pipelines, etc. as more experimental data becomes available.

The likelihood of resonant lock-on or strumming for a cable (or the absence of it) can be estimated from either Eq. (16) or Eq. (18). Kim et al (31, 32) had estimated two cases—a 290 m (950 ft) cable employed in field tests at St. Croix, and a 22.9 m (75 ft) cable employed in earlier field tests at Castine, ME (25, 26). Similar estimates can be made using a simplified form of Eq. (16); that is

$$\frac{\Delta\bar{x}}{\lambda_j} = 0.7\left(\frac{L}{D}\right) St\left(\frac{V^2}{\Delta V}\sqrt{\frac{m'}{T}}\right), \tag{16a}$$

and the results are compared in Table 4. Comparable conclusions can be drawn from the results of either equation—in the case of the long cable resonant strumming vibrations are unlikely, as estimated here and reported in Ref. (31, 32); in the case of the short cable resonant strumming vibrations are more likely, again as estimated here and reported in Refs. (26, 31, 32). The likelihood of the occurrence of resonant strumming vibrations can be estimated by comparing the cable length relative to

Table 4

Estimation of Cable Strumming in a Shear Current

Cable Properties from Refs. (26, 31, 32).

Experiment	Length/Diameter, L/D	Excitation Length/ Wavelength† $\Delta\bar{x}/\lambda_j$	Modal Frequencies per Bandwidth,†† N_S	Likelihood of Strumming
St. Croix (31, 32)	L = 290 m, D = 4.1 mm L/D = 7.1 (10^4)	~50	158	Random or no strumming.
Castine (26, 31, 32)	L = 22.9 m, D = 31.8 mm L/D = 720	~10	0.3	Non-lockin and resonant strumming.

†From Eq. (16a).
††From Eq. (18).

the expected strumming wavelength or the number of natural frequencies excited within the excitation bandwidth. The same conclusions follow from either approach.

7. MARINE APPLICATIONS

The hydrodynamic drag data given earlier in the report can be used to calculate the deflection of and forces on cylindrical structures in steady currents. A simple example of the problem of vortex-induced crossflow vibrations of a cylindrical beam in water is given in the Appendix. The method described there has been used previously by Every, King and Griffin (12) to compare predicted in line steady tip deflections of a model free-ended piling with the results of model experiments (8, 21). The drag amplification data given in Fig. 5 were employed in the previous comparison. In this section of the report a comparison is made using the up-dated and more extensive drag amplification results given here in Fig. 7.

The cantilevered circular cylinders employed in the experiments were models of the free-ended foundation piles for the Cognac field platform described by Fischer, Jones and King (20). Four cylinders of relative density γ = 1.5, 2.0, 2.5, and 3.5 were tested. Here the relative density is

$$\gamma = \frac{m_s + m_a}{m_a}, \tag{19}$$

where m_s is the physical mass (per unit length) and m_a is the fluid added mass. The properties of the cylinders are summarized in Table 5. Complete data sets consisting of the vortex-induced cross flow amplitudes of displacement and steady in-line deflection are available as a function of incident flow velocity (and reduced velocity V_r) for each of the four cylinders (12, 21). Two examples are given

here, for the cylinders of relative density $\gamma = 2.0$ and 2.5. The two cylinders exhibit quite different forms of response to the hydrodynamic forces.

Table 5

Vortex-Induced Vibrations of a Free-Ended Pile;

Properties for Figs. 9 and 10, from King (21).

Property	Model Value	Scale Factor (Fullscale/Model)
Length, L	0.66 m (2.17 ft)	168
Diameter, D	1.27 mm (0.042 ft)	168
Stiffness, $G = 3EI/L^3$	29.3 N/m (2.01 lb/ft)	168
Structural mass, m_S	0.061 kg/m (0.041 lb_m/ft)	168
Log decrement, δ	0.063	1
In-air natural frequency, f_n	8.75 Hz	$1/\sqrt{168}$

Note: The relative density γ of the basic pile model was varied by filling it with various substances.

Equation (A8) was evaluated for these two cases using corresponding values of $\overline{Y}_{MAX}$, $\overline{Z}_S$ and V_r. The results obtained are plotted in Figs. 8 and 9 where the experimentally-obtained values are shown together with two predictions. The dashed line represents the deflection $\overline{Z}_S$ that is predicted when the cylinder is restrained from vibrating, that is $C_D = C_{D0} = 1.2$, a constant value. The deflection predicted with Eq. (A8) is given by the solid line connecting the closed symbols. The prediction is in reasonable agreement with the experiment, similar to the agreement which was obtained previously by Every et al (12). Again there is a tendency to overpredict the steady deflection at lower reduced velocities, and displacement amplitudes, and to underpredict at the higher. The new drag prediction from Fig. 7 is less conservative than the prediction estimate used previously (12). The previous prediction estimate, using $A_1 = 0.54$ and $B_1 = 0.88$, is in fact an upper bound to the data shown in Fig. 7.

Only the lock-on range is shown in Fig. 8. Below and beyond the range of reduced velocities shown in the figure the measured deflections follow the dashed curve when the vortex-induced vibrations are negligible. There the cylinder is effectively stationary. In the range of $V_r = 5$ to 10 the drag force is amplified substantially by the vibrations and the deflection departs from the dashed line, reaches a maximum, and then returns to the dashed line. The effective drag coefficient averaged over

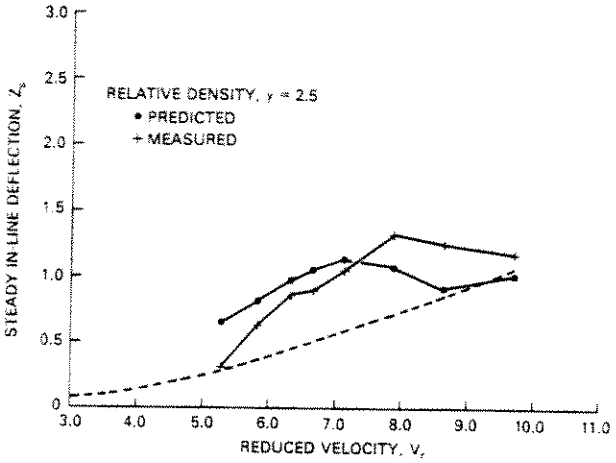

Fig. 8 — The predicted steady tip deflection $\bar{z}_s/D$ using Eqs. (9) and (A8) compared to the measured values from Every, King and Griffin (12). The predictions using a constant $C_{D0} = 1.2$ are shown as a dashed line. Relative density, $\gamma = 2.5$.

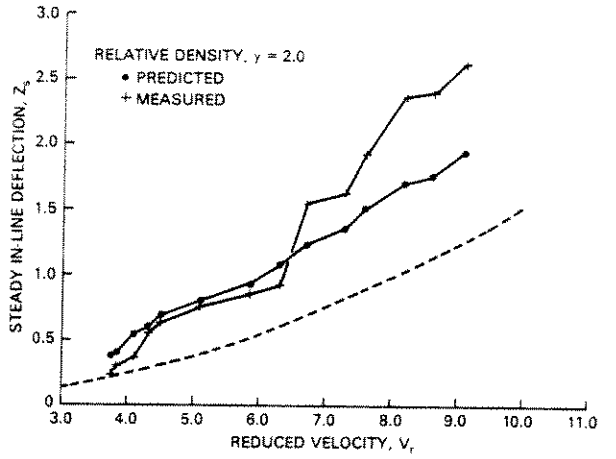

Fig. 9 — The predicted steady tip deflection $\bar{z}_s/D$ using Eqs. (9) and (A8) compared to the measured values from Every, King and Griffin (12). The predictions using a constant $C_{D0} = 1.2$ are shown as a dashed line. Relative density, $\gamma = 2.0$.

the length of the cylinder is increased to the range $C_D = 1.8$ to 2 at the largest tip amplitudes of $\bar{Y}_{MAX} = \pm 1.4$ D. This results in high steady stresses when the oscillatory stresses also are highest.

A different type of vortex-induced response is shown in Fig. 9. For this case the cylinder has a relative density of $\gamma = 2.0$, which corresponds to a cylinder of neutral buoyancy if the added mass of the cylinder is equal to the displaced mass of water. This is a reasonable assumption under most circumstances. The steady tip deflection $\bar{Z}_s$ increases monotonically along with the cross flow amplitude

of displacement $\bar{Y}_{MAX}$ over the reduced velocity range of $V_r = 4$ to 9. The displacement amplitude never reaches a maximum and then decreases toward the stationary state, so that the steady tip deflection of the free-ended pile increases in a corresponding way. The near-neutral buoyancy of the model may have increased the range of the oscillatory motion to incident flow velocities larger than those capable of being achieved during the experiment. A broad range of V_r over which the vortex-induced resonance occurred had been found in the case of near-neutrally buoyant models of the cold water pipe for ocean thermal energy conversion (OTEC) plants (34).

Similar applications to the problem of marine cable strumming vibrations have been made by Skop, Griffin and Ramberg in an analysis of the flow-induced motions of the SEACON II experimental mooring (19). More recently, McGlothlin (35) and Griffin and Vandiver (25, 26) have predicted the drag on model cables and pipe segments which were deployed during the field experiments conducted at Castine by MIT. The predicted drag on the strumming cable was somewhat below the measured drag (26, 35), but the predicted drag on the oscillating pipe segment was virtually indistinguishable from the measured drag (25, 35). The prediction curve given in Fig. 5 was employed in these earlier estimates of the vortex-induced drag coefficient. However, comparable agreement also has been obtained using the up-dated Eq. (9). Some examples are given in Table 6 where the drag has been estimated using the equation

$$C_{DT} = C_{DO}[1.16 + 1.67(\bar{Y}_{rms}/D)]. \tag{20}$$

This equation represents the *spatial* average drag on a cable or pipe segment which oscillates normal to a uniform current with an amplitude of displacement from equilibrium of $\bar{Y}_{rms}$. The rms of the displacement amplitude $\bar{Y}$ in Table 6 is the instantaneous value of a moving average at a given time in the record. The original version of Eq. (20) was derived by McGlothlin (35) and subsequently corrected by Griffin and Vandiver (26).

Table 6
Vortex-Induced Hydrodynamic Drag and Cables and Pipe Segments
Comparison of Measured and Predicted Values

	Model		
	Coefficient, C_D ($\bar{Y}_{rms}$)†	Coefficient, C_D †	Coefficient, C_D ††
Bare Cable	3.01 (0.51 D)	2.51	2.41
	3.15 (0.47 D)	2.43	2.33
Pipe Segment	2.61 (0.52 D)	2.45	2.43
	2.43 (0.61 D)	2.51	2.61

†MIT experiments, from Refs. (25, 26, 35).
††From Eq. (20), this report.

The drag on the long cable was predicted by Kim using the measured values of $\bar{Y}_{rms}$ from his experiments in the original version of Eq. (20). The drag predicted in this way was close to, but slightly greater than, the drag coefficients measured by Shargel (24) under random vibration conditions in the laboratory and by Kim at sea by fitting an overall drag coefficient C_D to the predicted values of measured cable top tension and inclination angle. These laboratory and field measurements were in good qualitative agreement overall for $\bar{Y}_{rms} = 0.1$ in 0.4.

The examples discussed here have shown once again that the cumulative effects of superimposed steady and unsteady stresses due to vortex-induced vibrations must be included in any design assessment of proposed structures in water. There now exists a more extensive and directly applicable data base for hydrodynamic drag coefficients and displacement amplitudes, so that such an assessment is more straightforward and can be made with more confidence than before.

8. CONCLUDING REMARKS

The dynamic analysis of marine structures and cable systems has become increasingly important in order to predict stress distributions and operational lifetimes in hostile environments. This is largely because the amplitudes of vortex-induced vibration for a cylindrical structure such as a riser or pipeline in water are an order of magnitude greater than for a similar structure in air. The small mass ratio (structure to displaced fluid) in water produces small values of the reduced damping which in turn result in the relatively large limiting vibration amplitudes shown here in Fig. 2.

There is a relatively wide range of reduced damping over which bluff cylindrical structures in water undergo large-amplitude vibrations due to vortex shedding. Thus it is not possible to suppress these oscillations by means of mass and damping control, and some form of external device such as a helical strake winding or fairing usually is required. The exciting component of the lift force coefficient which drives the motion is increased by the vortex-induced vibrations until a maximum is reached, after which the exciting force approaches zero as the limiting amplitude of displacement is approached.

Risers, platform mooring cables and other long, slender structures often are subjected to spanwise non-uniform shear currents. The response of long cylinders in non-uniform flows cannot be predicted accurately in many cases using existing methods which were originally developed for uniform flows. There is a limited base of data available for current shear effects from both laboratory and field experiments. However, it is possible from these results to make reasonable engineering estimates of the level and extent of vortex-induced vibrations in shear currents. Several examples are given here in this report.

The vortex-induced hydrodynamic drag forces on vibrating structures in water are amplified substantially above the corresponding case of a structure at rest. This drag amplification has been measured in several extensive experiments and reaches 250 percent at the largest amplitudes of crossflow displacement. The available experimental results for circular cylindrical members are summarized here and put to use in several example calculations. This amplification of the hydrodynamic drag forces results in large steady stresses and deflections when the oscillatory stresses and deflections also are highest.

The cumulative effect of superimposed stresses must be considered in any design assessment of proposed structures in a marine environment where currents are a factor. Such an assessment now can be made with more confidence than was possible before.

9. REFERENCES

1. T. Sarpkaya, "Vortex-Induced Oscillations, A Selective Review," Trans. ASME, J. Applied Mechanics, Vol. 46, 241-258, 1979.

2. P.W. Bearman, "Vortex Shedding From Oscillating Bluff Bodies," Ann. Rev. Fluid Mech., Vol. 16, 195-222, 1984.

3. R. King, "A Review of Vortex Shedding Research and Its Applications," Ocean Engineering, Vol. 4, 141-171, 1977.

4. O.M. Griffin and S.E. Ramberg, "Some Recent Studies of Vortex Shedding with Application to Marine Tubulars and Risers," Trans. ASME, J. Energy Resources Tech., Vol. 104, 2-13, 1982.

5. O.M. Griffin, "Current-Induced Loads on Marine Structures due to Vortex Shedding," in *Proc. Ocean Structural Dynamics Symposium '84*," J.W. Leonard (ed.), Oregon State University, 457-471, September 1984.

6. R.A. Skop and O.M. Griffin, "On a Theory for the Vortex-Excited Oscillations of Flexible Cylindrical Structures," J. Sound and Vib., Vol. 41, 263-274, 1975; see also "The Vortex-Induced Oscillations of Structures," J. Sound and Vib., Vol. 44, 303-305, 1976.

7. W.D. Iwan, "The Vortex-Induced Oscillation of Elastic Structural Elements," Trans. ASME, Series B, J. Engrg. Indus., Vol. 97, 1378-1382, 1975.

8. M.J. Every and R. King, "Suppressing Flow-Induced Vibrations—An Experimental Study of Clamp-On Devices," BHRA Fluid Engineering Report RR 1576, November 1979.

9. G. Moe, Private communication, 1983.

10. D.T. Tsahalis, "Vortex-Induced Vibrations of a Flexible Cylinder Near a Plane Boundary Exposed to Steady and Wave-Induced Currents," Trans. ASME, J. Energy Resources Tech., Vol. 106, 206-213, 1984.

11. D.T. Tsahalis, "Vortex-Induced Vibrations Due to Steady and Wave-Induced Currents of a Flexible Cylinder Near a Plane Boundary," in *Proc. Fourth Int. Offshore Mech. and Arctic Eng. Symp.*, Vol. I, ASME: New York, 618-628, February 1985.

12. M.J. Every, R. King and O.M. Griffin, "Hydrodynamic Loads on Flexible Marine Structures due to Vortex Shedding," Trans. ASME, J. Energy Resources Tech., Vol. 104, 330-336, 1982.

13. M.M. Zdravkovich, "Review and Classification of Various Aerodynamic and Hydrodynamic Means for Suppressing Vortex Shedding," J. Indus. Aero. and Wind Engrg., Vol. 7, 145-189, 1981.

14. H. Adami and B.A. Batch, "Aeolian Vibrations of Tubular Busbars in Outdoor Substations," Electra, No. 75, 99-120, March 1981.

15. R.D. Blevins, *Flow-Induced Vibration*, Van Nostrand Reinhold: New York, 1977.

16. O.M. Griffin, "Vortex-Excited Cross-Flow Vibrations of a Single Cylindrical Tube," Trans. ASME, J. Press. Vessel Tech., Vol. 102, 158-166, 1980.

17. J.M. Simmons and P.M.G. Cleary, "Measurement of Aerodynamic Power Associated with Vortex-Induced Vibration of Electrical Transmission Lines," IEEE Power Engineering Society Paper F79 713-9, 1979.

18. F.B. Farquharson and R.E. McHugh Jr., "Wind tunnel investigation of conductor vibration with use of rigid models," Trans. AIEE, Vol. 75, 871-878, 1956.

19. R.A. Skop, O.M. Griffin and S.E. Ramberg, "Strumming Predictions for the SEACON II Experimental Mooring," Offshore Technology Conference Paper OTC 2884, May 1977.

20. F.J. Fischer, W.T. Jones and R. King, "Current-Induced Oscillations of Cognac Piles During Installation," in *Practical Experiences with Flow-Induced Vibrations*, E. Naudascher and D. Rockwell (eds.), Springer-Verlag: Berlin, 570-581, 1980.

21. R. King, "Model Tests of Vortex-Induced Motion of Cable Suspended and Cantilevered Piles for the Cognac Platform," BHRA Fluid Engineering Report RR 1453, January 1978.

22. T. Overvik, "Hydroelastic Motion of Multiple Risers in a Steady Current," Ph.D. Thesis, Norwegian Institute of Technology, August 1982.

23. T. Sarpkaya, "Transverse Oscillation of a Circular Cylinder in Uniform Flow," Proc. ASCE, J. WPCO Div., Vol. 104, 275-290, 1978.

24. R.S. Schargel, "The Drag Coefficient for a Randomly Oscillating Cylinder in a Uniform Flow," M.S. Thesis, MIT Ocean Engineering Department, September 1980.

25. J.K. Vandiver, "Drag Coefficients of Long, Flexible Cylinders," Offshore Technology Conference Paper OTC 4490, May 1983.

26. O.M. Griffin and J.K. Vandiver, "Flow-Induced Vibrations of Taut Marine Cables with Attached Masses," Naval Civil Engineering Laboratory Report CR 84.004, November 1983.

27. M.E. Davies and A.P. Daniel, "The Hydrodynamics of a Model of a Vibrating Umbilical Cable," Offshore Technology Conference Paper OTC 4832, May 1984.

28. O.M. Griffin, "Vortex Shedding From Bluff Bodies in a Shear Flow: A Review," Trans. ASME, J. Fluids Eng., Vol. 107, forthcoming, 1985.

29. A.K. Whitney and K.G. Nikkel, "Effects of Shear Flow on the Vortex-Shedding-Induced Response of Marine Risers," Offshore Technology Conference Paper OTC 4595, May 1983.

30. N.M. Patrikalakis and C. Chryssostomidis, "Vortex Induced Response of a Flexible Cylinder in a Shear Flow," *Proc. Fourth Int. Offshore Mech. and Arctic Eng. Symp.*, ASME: New York, February 1985.

31. Y.-H. Kim, J.K. Vandiver and R.A. Holler, "Vortex-Induced Vibration and Drag Coefficients of Long Cables Subjected to Sheared Flows," *Proc. Fourth Int. Offshore Mech. and Arctic Eng. Symp.*, Vol. I, ASME: New York, 584-592, February 1985.

32. Y.-H. Kim, "Vortex-Induced Response and Drag Coefficients of Long Cables in Ocean Currents," Ph.D. Thesis, MIT Ocean Engineering Department, October 1984.

33. O.M. Griffin, "Vortex Shedding From Cables and Structures in a Shear Flow: State-of-the-Art," Naval Civil Engineering Laboratory Report CR 83.004, November 1982.

34. O.M. Griffin, "Hydrodynamic Effects Due to Vortex Shedding From the OTEC Cold Water Pipe," *Proc. Second Int. Offshore Mech. and Arctic Eng. Symp.*, ASME: New York, 156-164, February 1983.

35. J.C. McGlothlin, "Drag Coefficients of Long Flexible Cylinders Subject to Vortex Induced Oscillations," M.S. Thesis, MIT Ocean Engineering Department, January 1982.

36. R.E.D. Bishop and D.C. Johnson, *Mechanics of Vibration*, Cambridge University Press: Cambridge, 1960; Chapter 7.

10. APPENDIX : CALCULATION OF DRAG-INDUCED MEAN IN-LINE DEFLECTIONS

It is possible to predict the steady deflection of the oscillating cylinder in Fig. 6 by treating it as a long, flexible beam since the cylinder has a length/diameter ratio of $L/D = 52$. The equation for the steady deflection $Z_s(x)$ of a simple, flexible cantilever can be written as

$$Z_s'''' = K\ C_D(x), \tag{A1}$$

where

$$K = \frac{3}{2}\ \frac{\rho}{g_c}\ \frac{V^2 L}{G}. \tag{A2}$$

The primes denote the derivative taken with respect to x, the direction along the cylinder. Here g_c is the gravitational constant and the stiffness $G = 3EI/L^3$. The steady deflection Z_s is measured in multiples of the diameter D and the displacement x (measured from the clamped end $x = 0$) is measured as a fraction of the length L. Tensile forces are neglected for this simple example, although in the case of more complex structures such as risers, conductor pipes, and cables the tension variation in the axial direction cannot be neglected in either static or dynamic analyses.

The distributed loading on the right-hand side of Eq. (A1) is due to the drag forces which vary locally with the vortex-induced vibrations along the cylinder. As shown earlier, the drag coefficient C_D (normalized by the stationary cylinder value C_{D0}) can be represented as a function of the response parameter

$$w_r = (1 + 2\bar{Y}/D)\ (St\ V_r)^{-1}. \tag{A3}$$

Both the reduced velocity $V_r = V/f_n D$ and the local displacement amplitude $\bar{Y}/D$ are accounted for in the expression for w_r. St is the Strouhal number for $\bar{Y}/D = 0$. For the purposes of this example the linear least-squares representation of the data in Fig. 7 is

$$C_D/C_{D0} = A_1 + B_1 w_r, \text{ with } A_1 = 0.124 \text{ and } B_1 = 0.933, \tag{A4}$$

as discussed in the report. Equation (A4), which in effect yields the dependence of the drag coefficient C_D on the vortex-induced displacement amplitude $\bar{Y}$ and the flow velocity V, can be expanded to

$$C_D = C_{D0}\{A_1 + B_1(1 + 2\bar{Y}(x)/D)\ (St\ V_r)^{-1}\}.$$

The fundamental normal mode of vibration of cantilever beam for this simple example is approximated reasonably well by (36)

$$y = \bar{Y}_{MAX}\left[1 - \cos\left(\frac{\pi}{2}x\right)\right], \tag{A5}$$

where the tip displacement is given by $\bar{Y}_{MAX}$. Equation (A4) then is of the form

$$C_D = C_{D0}\left\{A_1 + B_1A_2\left[1 + B_2\left(1 - \cos\left(\frac{\pi}{2}x\right)\right)\right]\right\}$$

where $A_2 = (St\ V_r)^{-1}$ and $B_2 = 2\ \bar{Y}_{MAX}/D$. Then the beam equation then takes the form

$$Z_s'''' = K_1 - K_2 \cos\left(\frac{\pi}{2}x\right) \tag{A6}$$

where $K_1 = K\ C_{D0}[A_1 + B_1A_2(1 + B_2)]$ and $K_2 = K\ C_{D0}\ B_1A_2B_2$. The appropriate boundary conditions for a cantilever beam are

$$Z_s(0) = Z_s'(0) = 0,$$
$$Z_s''(1) = Z_s'''(1) = 0.$$

It is assumed as a first approximation that any differences between the normal mode shape and the forced mode shape are negligible. King (21) has found that within reasonable limits cylinders oscillating due to vortex shedding do so in normal modes. This point also is discussed by Every, King and Griffin (12).

When Eq. (A6) is integrated four successive times and the boundary conditions are applied appropriately, the solution is

$$Z_s(x) = K_1\frac{x^4}{24} + K_2\left(\frac{2}{\pi}\right)^4\left[1 - \cos\left(\frac{\pi}{2}x\right)\right] - \left[K_1 - K_2\left(\frac{2}{\pi}\right)\right]\frac{x^3}{6} + \left[\frac{K_1}{2} - K_2\left(\frac{2}{\pi}\right)\right]\frac{x^2}{2}. \tag{A7}$$

The steady deflection at the tip in the fundamental mode is given when Eq. (A7) is evaluated at $x = 1$, or

$$Z_s = \frac{1}{8}\ K_1 - K_2\left[\frac{2}{3\pi} - \left(\frac{2}{\pi}\right)^2\right]. \tag{A5a}$$

In terms of the various coefficients in Eqs. (A4) and (A6), this latter equation becomes

$$Z_s = K\ C_{D0}\{0.125[A_1 + B_1A_2(1 + B_2)] - 0.048B_1A_2B_2\}. \tag{A8}$$

These equations are employed in two examples given in Section 7 of the report.

DEPARTMENT OF THE NAVY

NAVAL RESEARCH LABORATORY
Washington, D.C. 20375-5000

OFFICIAL BUSINESS
PENALTY FOR PRIVATE USE, $300

POSTAGE AND FEES PAID
DEPARTMENT OF THE NAVY
DoD-316
THIRD CLASS MAIL